Reconfigurable Elastic Metamaterials

Willa Yunqi Yang*", Yumeng Zhuang*, Luke Darcy*, Grace Liu*, Alexandra Ion*
{yunqiy,yumengzh,ldarcy,gmliu,aion}@andrew.cmu.edu
*Human-Computer Interaction Institute, School of Computer Science, Carnegie Mellon University
Pittsburgh, PA, USA
"University of Chicago
Chicago, IL, USA

Figure 1: We propose a reconfigurable metamaterial that can be easily and repeatedly reconfigured by end users. We envision (a) that the generic material sheet can be purchased as larger sheets, and be cut and configured to opportunistically augment the elastic properties of objects. We show how this material can be applied to realize applications, such as (b) passive haptic props for VR, (c) custom shoe soles or (d) piano keys.

ABSTRACT

We present a novel design for materials that are reconfigurable by end-users. Conceptually, we propose decomposing such reconfigurable materials into (1) a *generic, complex* material consisting of engineered microstructures (known as metamaterials) designed to be purchased and (2) a *simple* configuration geometry that can be fabricated by end-users to fit their individual use cases. Specifically, in this paper we investigate reconfiguring our material's *elasticity*, such that it can cover existing objects and thereby augment their material properties. Users can configure their materials by generating the configuration geometry using our interactive editor, 3D printing it using commonly available filaments (e. g., PLA), and pressing it onto the generic material for local coupling. We characterize the mechanical properties of our reconfigurable elastic metamaterial and showcase the material's applicability as, e.g., augmentation for haptic props in virtual reality, a reconfigurable shoe sole for different activities, or a battleship-like ball game.

CCS CONCEPTS

• **Human-centered computing** → **Interactive systems and tools**.

This work is licensed under a Creative Commons Attribution International 4.0 License.

UIST '22, October 29-November 2, 2022, Bend, OR, USA
© 2022 Copyright held by the owner/author(s). Publication rights licensed to ACM.
ACM ISBN 978-1-4503-9320-1/22/10.
https://doi.org/10.1145/3526113.3545649

KEYWORDS

metamaterials, reconfigure, fabrication, 3D printing, elasticity, programmable matter, HCI

ACM Reference Format:
Willa Yunqi Yang*", Yumeng Zhuang*, Luke Darcy*, Grace Liu*, Alexandra Ion*. 2022. Reconfigurable Elastic Metamaterials. In *The 35th Annual ACM Symposium on User Interface Software and Technology (UIST '22), October 29-November 2, 2022, Bend, OR, USA.* ACM, New York, NY, USA, 13 pages. https://doi.org/10.1145/3526113.3545649

1 INTRODUCTION

Additive manufacturing, such as 3D printing, offers the freedom to freely arrange material in space, enabling custom objects of higher complexity. Taking advantage of the capability to fabricate complex geometry, researchers started designing microscale structures that together form unique material properties, i. e., they started engineering the material rather than the object. Such artificial structures, often arranged on a grid, are known as mechanical metamaterials.

Metamaterials enable engineering unique material properties and researchers demonstrated those by creating materials that can change their volume [45], absorb shocks [13, 47], provide local stiffness control [46, 48], or mechanically cloak objects [6]. To enable these properties, the materials consist of a lattice with many carefully designed unit cells with tuned parameters, i. e., their geometry is customized to achieve their bulk properties. Customization often results in one-off designs that are defined before fabrication.

Striving to go beyond pre-defined objects and materials, researchers investigate metamaterials that can be configured *after* fabrication. Structures allowing manual, cell-wise reconfiguration [16, 52], automatic shape change in rigid structures [2, 51], or robotic reconfiguration of material properties [10] have been demonstrated. However, these approaches require a stationary machine for reconfiguration and prevent in-situ adaptation or are not easily repeatable because of their manual configuration process.

In this work, we propose reconfigurable metamaterials for *end-users*. Our metamaterial can be repeatedly configured after fabrication in-situ and extends prior work in that the configuration interaction is designed to be simple, quick, and accessible to makers, yet enabling well-defined, locally tunable, dynamic material properties.

Conceptually, the main idea behind our user-definable reconfigurable metamaterials is that the *complex* micro-structured material is *generic* and can be produced by industry, while the *specific* configuration mechanism is *simple* and trivial to fabricate by users at home. As illustrated in Fig. 1a, we envision that users would purchase this generic material in stores as a stock material in the future. A software tool would allow them to specify its local material properties and export the simple geometry, which users print and snap onto the generic material to configure larger areas at once. While this concept can potentially be applied to a variety of materials, in this paper we specifically investigate a reconfigurable metamaterial with locally tunable *elasticity*.

Specifically, we design a generic elastic metamaterial that contains two types of unit cells: (1) a *spring cell* which returns kinetic energy and (2) a *damper cell* that absorbs it. Those cells are arranged in a checkerboard pattern throughout the material, making a generic material with evenly distributed cells, as illustrated in Fig. 2a-b. This yields a locally tunable elastic material *after fabrication.*

The material can be configured by printing *configuration layers*. We designed the geometry of the configuration layer to be simple to enable users to 3D print it at home using readily available materials, such as PLA. Fig. 2c shows 3 different configuration layers as examples. These layers have hooks at selected positions. As shown in Fig. 2d, when users press the lid onto the material, the hooks engage with the cells at selected locations to activate a subset of cells that contribute to the elastic response of the material locally. Note that the material can be covered by multiple, different configuration layers to employ locally varying user-defined elasticity. An area can be configured to return most of the kinetic energy introduced by the impact of a ball, resulting in a high bounce back. Another area on the same material can be configured to absorb most of the energy of the falling ball, which exhibits only a low bounce back.

We support users in reconfiguring the material with our configuration tool that we will discuss later in this paper. This tool generates the configuration layer based on users' high-level specifications, including area, target bounce back, and approximate mass.

1.1 Contributions

The main contribution of this work is a generic elastic material that can be configured repeatedly by end-users. This enables users to reapply the material to different objects and thereby reuse it for different purposes. The specific contributions of this paper are the following:

(1) *Interaction design for end-users.* Our reconfigurable metamaterial is explicitly designed with consumers as end-users in mind. We deliberately distinguish the complex generic material intended to be industrially manufactured from the simple specific configuration geometry that end-users print.
(2) *Mechanical design.* We contribute the mechanical design of such reconfigurable elastic metamaterials, including their technical evaluation and a Rhino-based[1] tool to support their configuration.
(3) *Exploration of applicability.* We demonstrate the utility of our elastic materials in several application examples to clarify their capabilities.

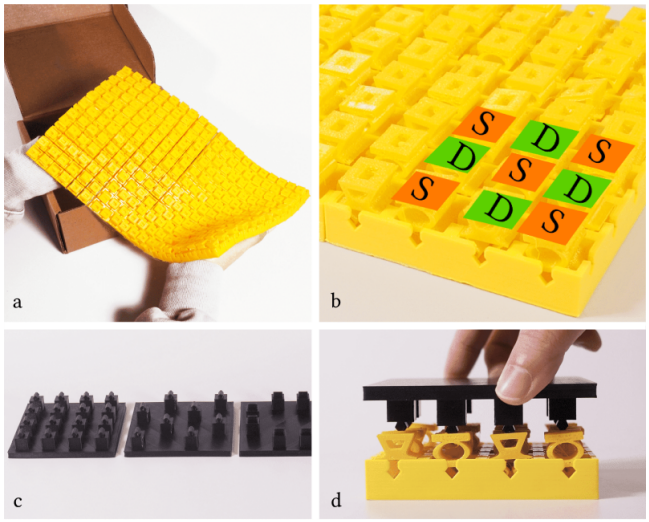

Figure 2: (a) We designed our metamaterial to be generic such that it can be mass-fabricated in the future. (b) It consists of two unit cells: spring and damper cells, arranged in a checkerboard pattern. Users can configure the material's elasticity by (c) coupling combinations of spring and damper cells. (d) The hooks on the coupling layers selectively engage with the unit cells to activate a subset which is effective in defining the elasticity of its connected area.

2 RELATED WORK

Our work builds on prior findings in personal fabrication using soft and dynamic elements and mechanical metamaterials.

2.1 Personal fabrication with compliant elements

While 3D printing allows for realizing objects with arbitrary geometry, the available materials are rather limited to plastics, the vast majority of which are rigid. To explore a broader range of materials for personal fabrication, researchers investigated techniques,

[1] https://www.rhino3d.com/

machines and design tools to create soft objects. These include machines that use soft base materials such as fabric [1, 21, 37, 41, 42], or techniques for printing thin fabric-like structures from rigid filaments [12, 50]. Insights from these techniques for printing soft structures from rigid materials were integrated with locally rigid parts to enable objects with locally varying compliance [26].

Beyond fabricating soft objects, researchers also set out to help users embed *dynamic* parts. He et al. [19] proposed a modeling system that embeds custom parametric coil springs into e. g., figurines for enhanced dynamic behaviour. Lamello [44] adds cantilever springs into common widgets, such as sliders or rotary knobs. They primarily use the sound produced by the cantilever springs for tracking the widget's value, but it also creates haptic feedback by construction. Chen et al. [8] proposed a computational design algorithm that generate the geometry for dynamic, e. g., jumping, structures automatically. Furthermore, systems that incorporate pneumatic actuation are inherently dynamic and have been shown in combination with 3D printing to enable large-scale kinetic structures [29], enable shape-change [34], or embed sensing capabilities [18, 49].

Most of these works define the functionality of the object before it is fabricated. We present a material, the dynamic properties of which can be repeatedly configured by users.

2.2 Mechanical metamaterials

Metamaterials are complex geometries, often designed as many unit cells arranged periodically, that surpass the material properties of their constituent parts [4]. In other words, the concept of metamaterials allows us to engineer novel materials rather than objects, by carefully designing their microstructure. Such metamaterials enable engineering unique material properties, such as materials that are ultra-lightweight [33], change their volume [30, 45], absorb shocks [13, 47], change their stiffness [46, 48], or mechanically cloak objects [6].

The majority of prior work on metamaterials is concerned with creating new materials, i. e., engineering the bulk properties of a material. Only recently, researchers started investigating materials with engineered *local* properties that have been shown to assume mechanisms and robotic movement [22, 24], employ computation [25], allow sensing capabilities [14, 43], change their outside and internal structures post-fabrication [23, 28], or deploy to pre-defined shapes [7, 32].

The reconfigurable metamaterial that we propose in this work is elastic, therefore the works most closely related employ varying stiffness and shock absorption. Locally variable stiffness materials have been shown as simple geometries, such as holes [5], foam-like structures [31], or more complex geometries [9, 36, 46]. Shock absorbing structures were shown using bistable elements that trap energy after they snap through [13, 47]. While we considered using bistable structures, they effectively introduce a threshold of force after which they trap energy, while for smaller forces they would act as springs. Additionally, all our cells are designed to be printed in an un-coupled state such that they can be coupled after fabrication selectively based on users' needs.

2.3 (Re-)Configurable materials

While the geometry and therefore the function and properties of the majority of metamaterials are defined before fabrication, researchers very recently started investigating materials that can be configured later. One example is a cut kirigami pattern that is configured by being pulled apart, causing the sheet to buckle and the spikes to pop out, making for a snake robot skin with increased friction [38]. The configuration is not reversible. Metamaterials with actuated bulk properties have been demonstrated using pneumatic [35, 53] and magnetic actuation [15]. Some metamaterials have been proposed that can change their shape after fabrication by locally and manually switching bistable springs [11, 16], or sculpting the heated, pliable structure into shape [52]. The manual reconfiguration process limits the precise repeatability. Preprogrammed shape-changing objects have been demonstrated as rigid objects [2, 51]. The most closely related work are reprogrammable elastic materials that are configured using a custom machine that actuates embedded magnets within the cells to change elasticity locally [10].

In our work, we extend this area and contribute structures that can be configured repeatedly with the same precision by end-users.

3 MECHANICAL DESIGN OF RECONFIGURABLE CELLS

As we illustrated in Fig. 2, our generic elastic metamaterial consists of two types of cells arranged in a checkerboard pattern. The cells can be coupled locally and selectively to configure the material's elasticity. In this section, we will describe the mechanical design of the cells and the configuration layer for our basic metamaterial.

3.1 Spring Cell

The spring cells within our metamaterial are designed to store and return energy. Traditional springs are typically made from hardened steel, the high rigidity and elastic range of their base material is a main contributor to their elastic behavior. The goal of our metamaterial is to embed springs *and* dampers made from the same, easy-to-manufacture material, which we prototype using the rubber-like filament *Ninjaflex*. We engineered the geometry of the spring to achieve the desired stiffness. In the following exposition, we use cell size with a square base of 22.5 mm. We refer to different scales in Section 6.

As illustrated in Fig. 3, the design of our spring cell is a double-layered, stacked oval. We landed on the stacked oval design after experimenting with different geometries including zigzags, pantographs, ovals, etc. In order for the spring to store more elastic energy, we empirically engineered the ovals to feature thicker edges. We found that when the spring deforms and flattens, the thicker edges can store more elastic energy and spring back more easily. For the depicted cell in Fig. 3, the thickness ratio is 2:1, compared to the thickness of the base oval. This resulted in a measured spring stiffness of approx. 1800 N/m, which we measured using a 50 N force gauge with 0.2% accuracy. Although our spring is made from a hyperelastic material [39], our measurements support that it can be approximated as a linear, Hookean spring. We elaborate on this in our technical evaluation in Section 5.

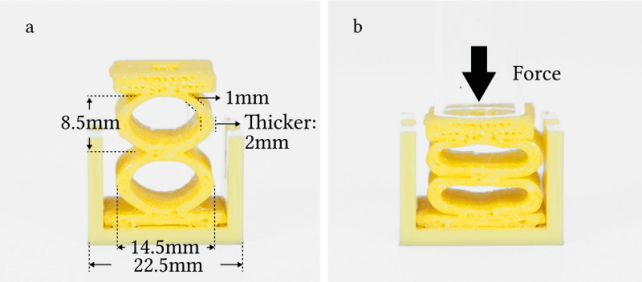

Figure 3: Our spring cell geometry consists of two stacked ovals with varying thickness for elastic energy storage. From its (a) rest state, it can be (b) compressed by 9 mm.

3.2 Damper Cell

The purpose of our damper cells is to absorb shock by reducing the energy returned to a colliding object. Our damper design implements Coulomb damping [40] where energy is absorbed through dry friction. We chose dry friction as it provides room for us to tune the energy dissipation to damp impacts of different sized masses linearly, including very small masses (32g). When a mass impacts a damper cell, as we show in Fig. 4, it will compress causing its top to slide against the frame. The frame wall is intentionally corrugated to increase friction, which dissipates kinetic energy by converting it to thermal energy. When the load is removed, the elastic zigzag legs push the top back out to allow repeated damping. We fine-tuned the thickness of the legs such that they are just elastic enough to return the top to its original height when the load is removed.

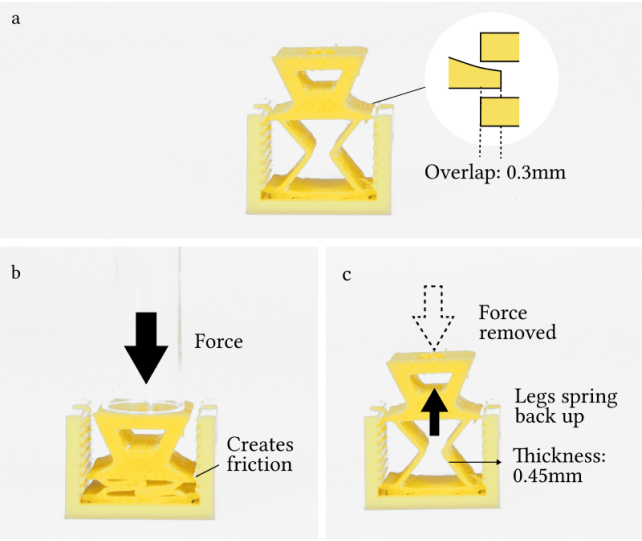

Figure 4: Our damper cell implements Coulomb damping, i. e., it uses sliding friction for energy dissipation. From (a) the rest state, it can be (b) compressed by 9 mm while dissipating energy through friction. The cell core (c) springs back to its original position after the force is removed.

Damper cells have lower and upper boundaries between which they can be the most effective. For very small impacts, the damper cell will resist compression and therefore sliding friction, resulting in no energy dissipation. For large masses, the distance that the cell top can travel might not be sufficient to dissipate most of the energy, resulting in smaller damping effects.

To increase the range of masses for which our damper cells are effective, we fine-tuned the overlapping distance between the cell top and the friction wall such that it is effective for masses larger than 32 g for our 22.5 mm cell configuration. For the upper boundary, the damping capacity of the material sheet can be increased by increasing the total number of damper cells to accommodate for larger masses, detailed in Section 5.

3.3 Configuration Layer

In our material, we define that a cell can have two states: *active* or *inactive*, and the configuration layer can activate cells or keep cells inactive. A layer consists of coupling lids which users can print at home using PLA. As illustrated in Fig. 5a, each unit area on a coupling lid can hold a hook to engage with a cell or omit it, rendering the cell inactive. The hook can be snapped onto the top of a cell to activate a cell. The design of the hook allows it to attach easily. Once snapped on, the lid will move with the cells.

Fig. 5c shows the configured material in its rest state. When a force is acting on the lid, the area with a hook will press down on the cell below it while a flat lid can keep the cell below it inactive. The length of the hook is equal to the maximum possible travel distance (9 mm) of a cell so that the inactive cells are not affected by the lid movement, while active cells can reach maximum compression. We illustrate this in Fig. 5d, showing that the two active cells have reached their maximum compression while the inactive cell in the middle remains in its rest position.

Selectively activating damper and spring cells using the configuration layer enables custom local elastic properties. To assist users in defining the necessary configuration for their desired elasticity, we implemented an online editor which generates the geometry upon high-level input, as we describe in Section 5.4

3.4 Note on Prototyping, Fabrication and Materials

Note that the geometry of the generic metamaterial in yellow is designed to be fabricated in one piece. For prototyping purposes, we 3D printed the cells and frames separately. Our prototypes were 3D printed using the off-the-shelf filament *Ninjaflex*[2], which is a rubber-like thermoplastic polyurethane. Some frames were printed using yellow PLA to speed up fabrication time. We did not find that the material choice for the frames had a significant impact on the configured elastic response. All prototypes are fabricated using consumer-grade printers, i. e., Ender 3, Ultimaker 2+, and Anycubic Mega S. All parts printed in *black* PLA filament[3] are intended to be fabricated by users, all parts in yellow are generic and intended to be mass-fabricated. Note that users *can* print the yellow parts at home, however since our generic metamaterial sheet has complex flexible internal structures, it prints very slowly at

[2]https://ninjatek.com/shop/ninjaflex/
[3]https://www.hatchbox3d.com/collections/pla-1-75mm

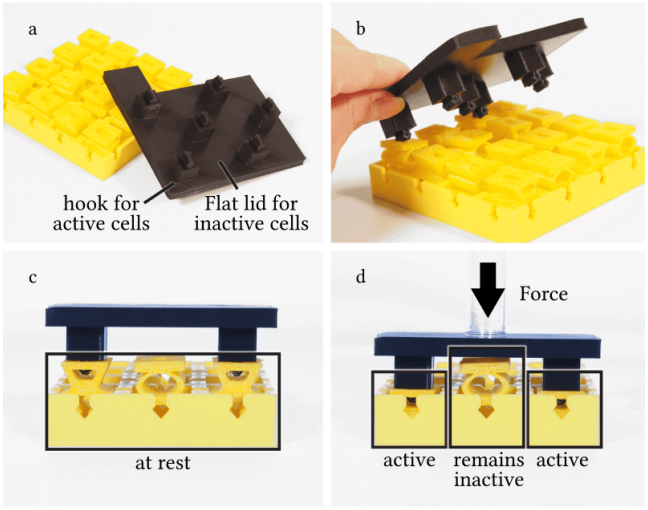

Figure 5: The coupling lid consists of (a) hooks for active cells and flat areas for inactive cells. (b) Users can simply press and snap the hook onto the cells for configuration. Cells will be (c) at rest when there is no force applied. When there is a force, (d) cells with a hook will travel up or down while cells without a hook remain inactive.

about 20mm/s. This takes approx. 63 hours for a 6×6 sheet—a burden to end-users. Therefore, our main contribution is to create a generic stock material that can be purchased in the future and configured by end-users.

4 APPLICATION EXAMPLES

We present four application examples to showcase different features of our material and application areas. Our material enables hands-on, in-situ prototyping of custom materials and objects. In the following, we outline applications that benefit from these properties, including in-situ creation of passive haptic props for VR applications, or enabling users to explore dynamic properties for shoes or instruments.

4.1 Augmenting Passive Props for Virtual Reality

Our reconfigurable elastic metamaterials can be applied to passive props in virtual reality scenarios to enhance tactile interaction. Complementary to dynamic VR haptic feedback devices, such as hand-held controllers that contain actuators and control circuits, *passive* haptic props are a well-established research area with the benefit that they reduce complexity by omitting actuators and their control (e.g., [3, 20]).

Passive haptic props often focus on matching only the shape of the real-world object (e.g., a cylinder) to the virtual object (e.g., a bottle). We demonstrate how users can utilize our material to enhance tactile interaction for hands-on, in-situ configuration of *elastic material properties* for passive props. To that end, we show a scenario in Fig. 6a where a user watches a movie in VR. We utilize our material to mimic 3 different objects, i.e., a sofa, a pump, and a remote control for the user to interact with during a 3D movie. Instead of using embedded circuitry [14], we use Oculus' built-in hand tracking to illustrate the applicability of our novel materials.

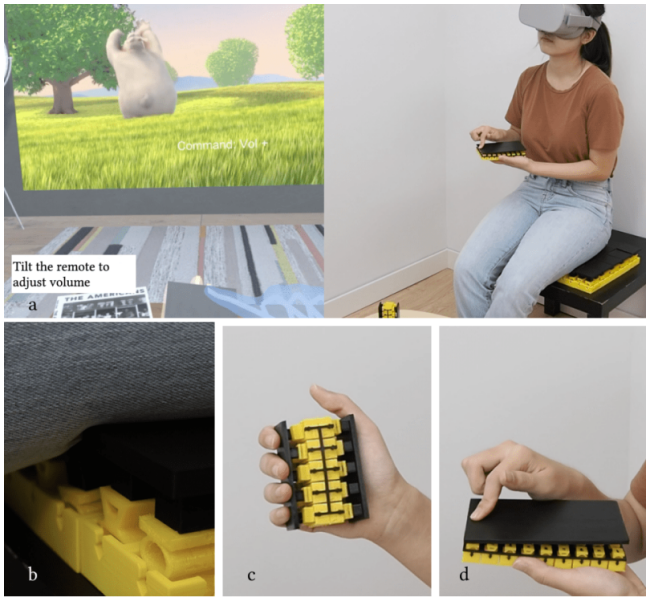

Figure 6: (a) The user is watching a VR movie with tactile props made from our material, including (b) a simulated sofa, (c) a pump to adjust the screen size, and (d) a remote control to adjust volume and playback speed. We use Oculus' built-in hand tracking to track the hand motions when interacting with the passive props.

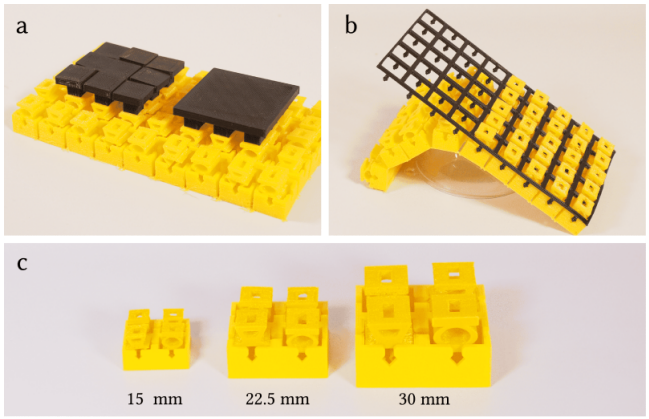

Figure 7: General configuration possibilities for our material include (a) varying the softness of a material by using individual configuration lids and omit coupling them, (b) snapping a thin deformation lock onto the initially flexible material, and (c) obtaining the generic material in different scales to span ranges of loads from fine-grained to human-scale.

(1) Sofa prop. In our scenario, the user first sits down on a virtual sofa. In reality and as shown in Fig. 6b, the sofa is a piece of our material configured to be compliant resting on a small rigid table—this shows how our material enables creating ad-hoc props. To do that, each cell received it's own lid, i.e., the cells remained uncoupled for maximum compliance, as shown in Fig. 7a. Only the sides of the sofa cushion are coupled to add additional support, similar to car seats. Since the sofa cushion is made for human-scale loads, we used larger cells, i.e., 30 mm, as shown in Fig. 7c. The resulting sofa cushion has approximately the size of a conventional sofa cushion. It can be reconfigured for other purposes or VR scenarios.

(2) Hand pump prop. Next, the user finds that the screen is too small in our VR scenario. They use the previously prepared hand pump prop to inflate the screen, as shown in shown in Fig. 6c. Fig. 8 shows the steps how the pump was prepared: after cutting a 5×4 cell patch from the deformable material sheet, users fold it over (Fig. 8a) and fixate the fold using a deformation lock (Fig. 8b) that snaps into the pre-defined holes and holds the material in shape. After adding configuration layers on both sides, users squeeze the double-side pump prop to adjusts the size of the VR screen (Fig. 8c)

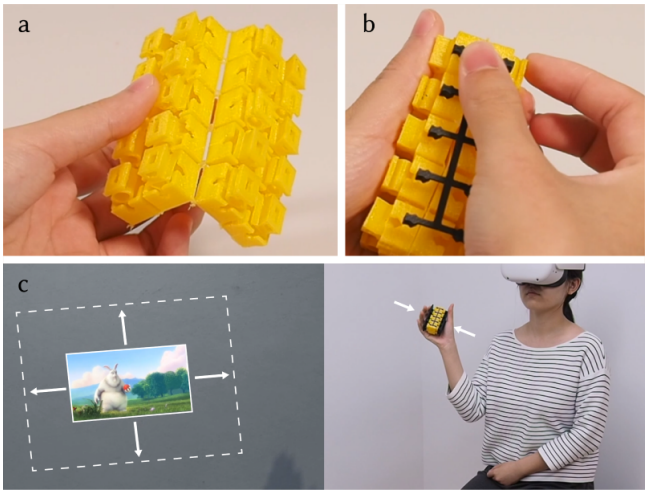

Figure 8: The hand-pump prop for our VR scenario is cut out of the deformable material, (a) folded over and (b) locked in place. After applying the coupling lids on both sides, (c) users squeeze the pump to increase the VR screen size.

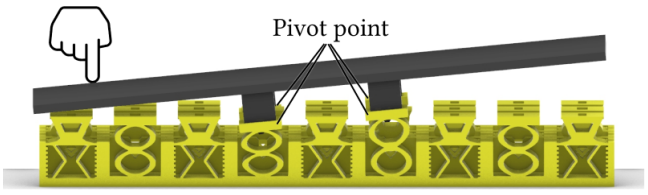

Figure 9: The material can be configured to tilt with the center springs as the pivot point.

(3) Remote control prop. Lastly, users increase the volume of the movie using our remote control prop, shown in Fig. 6d. Similar to how the pump is made, the remote sheet is cut from a larger deformable material sheet and locked in place using a deformation lock (Fig. 7b). The material is configured to tilt in four directions with the center as the pivot point; tilting up/down controls the volume, tilting left/right scrubs through the video. We show the simple tilting mechanism in Fig. 9. Note that the focus of this paper is on the structures and this VR scenario simply illustrates the different configuration possibilities enabled by our material.

4.2 Reconfigurable Shoe Sole

We envision that users can buy a generic shoe and reconfigure the shoe sole for different physical activities. We demonstrate two use cases in Fig. 10: long-distance running and playing volleyball.

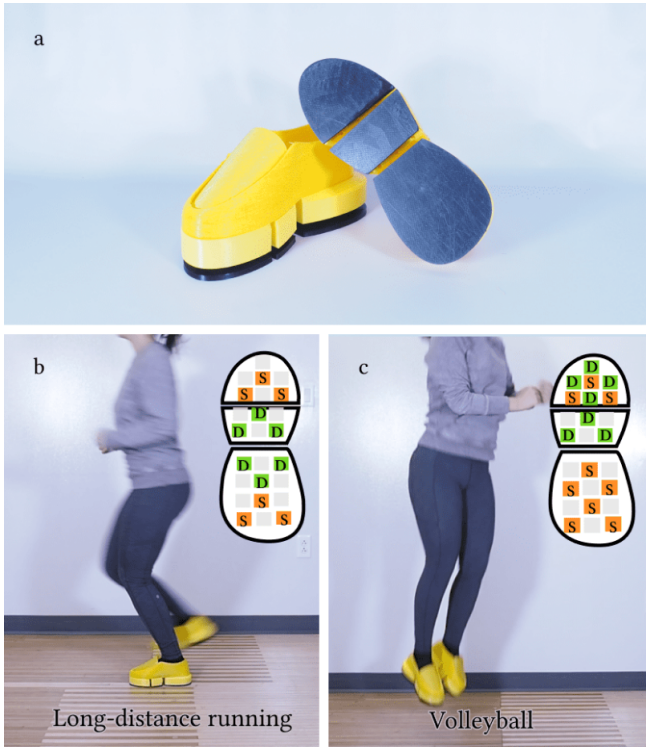

Figure 10: (a) Users can buy a generic shoe and reconfigure the shoe sole for different physical activities: (b) long-distance running; (c) playing volleyball.

Midfoot strikes are common in long-distance running[4]. As shown in Fig. 10b, we activate more damper cells in the middle area of the sole to act as shock absorbers to alleviate midfoot strikes. We also activate springs near the toes and heel of the foot for some amount of momentum.

Different from long-distance running, volleyball players tend to land jumps on the balls of their feet before planting their stance[5].

[4]https://www.roadrunnersports.com/blog/running-foot-strike/
[5]https://jvavolleyball.org/landing-paradox-training-volleyball-players-jump-land/

Landing flat-footed can lead to injuries such as muscle strain. Therefore, in the configuration for volleyball players shown in Fig. 10c, there will be a combination of springs and dampers on the ball of the foot for the purpose of more powerful attacks and safer landings. Active dampers in the midfoot can add cushioning when landing and springs on the heel can add more springiness.

We envision that shoe soles made of our reconfigurable elastic metamaterials can be connected to any generic shoe to perform needed tasks, lowering costs while also providing personal configurations. While this application example is not tuned to the wearer's weight and movement patterns, we demonstrate that the concept is applicable and could be adapted in the future.

4.3 Piano with adjustable key stiffness

Our material also affords multi-layered tilting. As demonstrated in Fig. 11, the piano's black and white keys are implemented on the same material sheet while having different hook heights to allow multi-layered tiling. If a piano is shared in a household, family members from children to adults can also customize their own desired key stiffness. The stiffness of the piano keys can also be configured non-uniformly, e. g., to support users with motor impairments in only one hand.

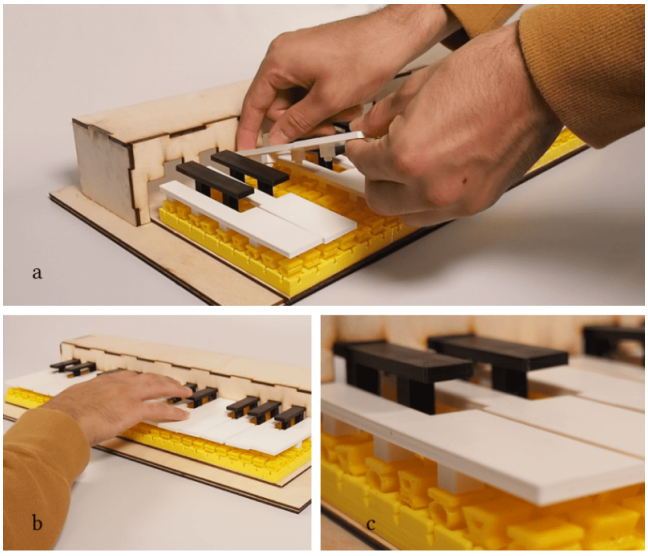

Figure 11: (a) Users can change piano keys and (b) play the piano on the material with customized key stiffness. (c) The feature of multi-layered tilting allows the height difference between black and white keys.

4.4 Ball game

Lastly, we demonstrate an battleship-style ball game that can be played on our large-scale material, as shown in Fig. 12. The goal of the game is for a player to catch more balls that bounce from the material than their opponent. Players configure the opponent's half with locally varying elasticity values by generating the corresponding configuration layers using our design tool. Since they configured the side, they know the elasticity values, but similar to a traditional battleship game, the map is concealed to their opponent. By intentionally throwing the ball onto areas with different elasticity, players leverage their knowledge about the bounce back behavior to make it difficult for their opponents to catch the ball. After a round is over, users can reconfigure the opponents sides by changing the location of the configuration lids to achieve a different map of elastic behavior for the next round.

Figure 12: A ball game that combines pong and battleship. (a) Users throw a ball onto the material, but could previously configure (b) the local elasticity to make it difficult for their opponent to catch the ball. The map is concealed as the configuration layer looks identical from the top.

5 ELASTICITY DEFINED BY CELL COMBINATIONS

We aim to understand how our material system performs when we couple cells across different areas. To do so, we collected experimental data, which we use to create a model to predict the elastic behavior and to use in our design tool. In this section, we describe our data collection procedure, show the raw data including visualizing the fit to our model, and derive the formulation.

5.1 Experimental Data Collection

To evaluate the dynamic response, we performed normal drop tests, similar to [17]. We used the test setup shown in Fig. 13, featuring transparent tubes with printed scales to guide the loads. We dropped different masses from a constant height of 330 mm onto the material. We used the tube with the inner diameter closest to the weight's diameter in order to guide the mass in the normal direction.

For all conditions, we used 4 different masses, i.e., 100, 200, 250, and 300 g. We varied the amount and composition of spring and damper cells, as we will illustrate in our results in the following. For each cell configuration, we used the smallest coupling lid that fits all cells in the present condition. We consistently started in

the center of the grid and placed cells radially outwards. We performed 3 repetitions for each mass-spring-damper configuration. For each trial, we recorded the mass bouncing and video-coded the first bounce back height in millimeters. Note that since uncoupled cells do not interact with each other and are modeled individually as simple Hookean springs and Coulomb dampers, we focus on investigating *coupled cells* for their complex combinational effects.

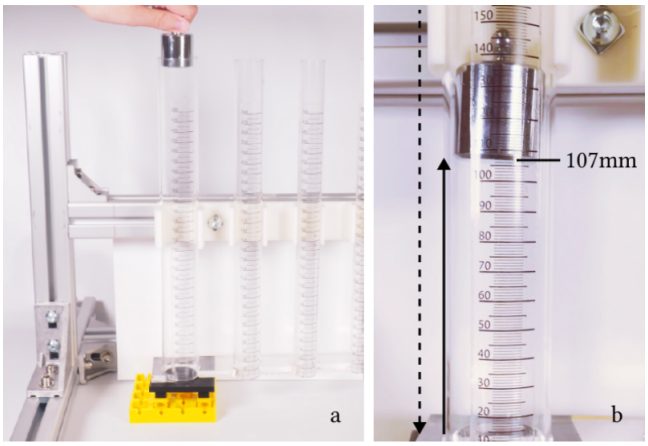

Figure 13: (a) Transparent tubes with printed scales were used to guide the loads. (b) Experiments were video-taped and peak bounce heights were recorded.

5.2 Results

For all results shown in the following, we illustrate the cell compositions on the left. We plot the average energy loss in Joules of our 3 trials along with error bars. Each graph displays the fit of our model as a dashed line. We derive the formulation of our model in the following section.

Vary only spring cells. First, we investigate the dynamic response when coupling multiple spring cells, without any damper cells present. We show the result of this experiment in Fig. 14. In this experiment, we test 6 different cell configurations, from 5 to 18 spring cells, with 4 masses and 3 repetitions each, yielding 72 trials. Our results show that the cells are effective in varying the energy dissipated after impact. We observe, however, that large masses cause the springs to saturate, i.e., compress them to their maximum, which limits the amount of elastic energy they can store. This is an important factor to be modeled in our formulation.

Vary only damper cells. Similarly, we aim to quantify the dynamics of coupling multiple damper cells. In this experiment, we activate only damper cells and no spring cells. Fig. 15 shows the conditions and results of this experiment. We tested 5 different configurations ranging from 4 to 18 damper cells, resulting in 60 trials (5 cell conditions × 4 masses × 3 repetitions). The lines are largely flat showing how our damper cells are effective in absorbing a lot of energy, which pushes the model towards maximum energy loss.

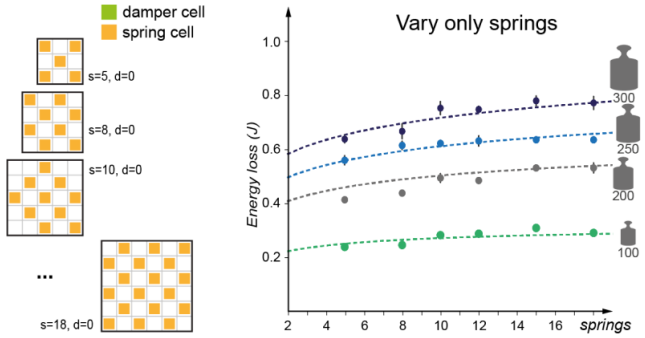

Figure 14: This graph shows the relationship between energy loss (J) and mass (g) for different number of spring cells. The scatter points with error bars show the measured data, while the dashed lines show the prediction of our model.

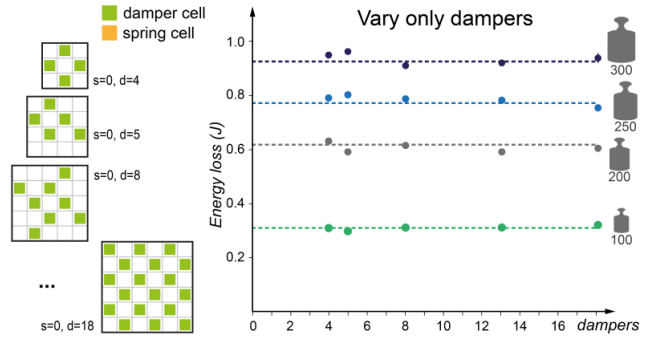

Figure 15: This graph shows the relationship between energy loss (J) and mass (g) for different number of damper cells. The scatter points with error bars show the measured data, while the dashed lines show the prediction of our theory. We find that the damper cells yield an approximately constant energy absorption across the cell configurations.

Constant springs, varying damper cells. To characterize the dynamic behaviour of coupling spring and damper cells, we set up an experiment with 9 springs being fixed. For each condition, we varied the number of damper cells. We illustrate the cell conditions and the results in Fig. 16. We tested 10 different configurations, where we added damper cells in the range from 0 to 18 to the existing 9 spring cells. This experiment resulted in 120 trials (10 cell conditions × 4 masses × 3 repetitions). The results, similar to that of varying spring cells only, confirm the constant nature of the dampers as we found in our aforementioned experiment.

Varying springs, fixed damper cells. Lastly, we add springs to a system of six dampers. We visualize the conditions and results in Fig. 17. This experiment resulted in 144 trials, as we tested 12 different cell conditions, ranging from adding 0 to 18 spring cells to the existing 6 damper cells. The results show that increasing the number of spring cells decreases the energy loss, as the springs offer energy storage and return energy when the material goes back

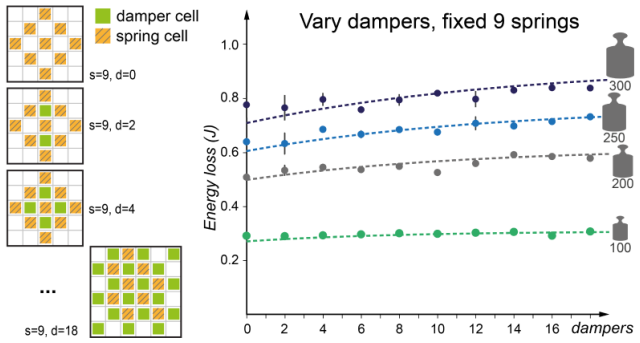

Figure 16: This graph shows the relationship between energy loss (J) and mass (g) for different numbers of damper cells while fixing the 9 spring cells. The scatter points with error bars show the measured data, while the dashed lines show the prediction of our model.

to its original shape. This effect decreases as the number of coupled cells increases.

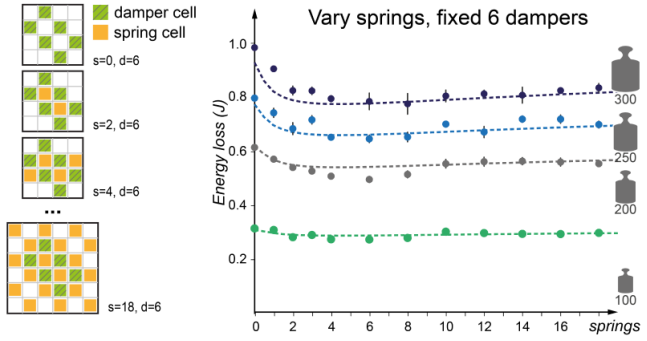

Figure 17: This graph shows the relationship between energy loss (J) and mass (g) for different numbers of spring cells while keeping the six dampers there. The scatter points with error bars show the measured data, while the dashed lines show the prediction of our model.

5.3 Formulation

We model the spring-damper mixture system as a damped harmonic oscillator [27] with varying spring and damping coefficients. Based on the model, we derive a formulation that approximates the expected elastic response. Since the formulation is complex, we fit the coefficients to experimental data using non-linear least squares fitting.

In the following, we will walk through the elements of our model and build it up from a simple mass-spring-damper system to the multi-component system with different combinations of damper and spring components.

For a *single* simple damped oscillator, the commonly used quality factor Q describes how well an oscillating system *preserves* energy [27]. To express the ratio of energy *dissipated* per cycle over the initial energy, we use the inverse of the quality factor Q, as illustrated by Fig. 18 and defined in the following:

$$\frac{1}{Q} = \frac{b}{\sqrt{mk}}$$

where we denote the load weight as m, the aggregate spring constant as k, and the damping constant as b.

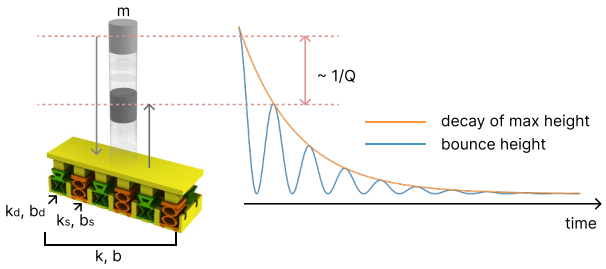

Figure 18: Energy dissipation in a damped harmonic oscillator in each cycle. Q factor reflects the decay rate of the bounce height. Left: Schematics of the experiment set up. k_s, k_d, b_s, and b_d are constants associated with the spring and damper cells, and they are combined into k and b of the whole system. Right: A sample graph showing the decay of the bounce height over time, and the highest starting point can be thought of as the drop height, and the first peak the first bounce height that we measure.

As we have *multiple* dampers and springs aligned on a surface, we approximate the system such that the unit cells share the same deformation. Therefore, the force acting upon the dropped mass during collision is the sum of that from all springs and dampers combined. As a result, the aggregate spring and damping constants are the sum of their individual spring and damping constants, respectively. If we have s springs, and d dampers, the aggregate spring constant is $sk_s + dk_d$, and the aggregate damping constant is $sb_s + db_d$. The subscript denotes which type of cell the constant belongs to, since springs and dampers have different properties. We label the constants on the corresponding cells in Fig. 18 for clarity.

Plugging these aggregate constants into the single element inverse Q equation yields

$$\frac{sb_s + db_d}{\sqrt{m}\sqrt{sk_s + dk_d}}.$$

Additionally, the collision of the falling mass with the configuration lid dissipates energy independent of the cells. To model that, we add a constant offset t to the equation above, which we determined by fitting the experimental data, yielding the following model:

$$x := \frac{sb_s + db_d}{\sqrt{m}\sqrt{sk_s + dk_d}} + t \tag{1}$$

At this point we should note that large numbers of springs or dampers can increase the stiffness to an extent where smaller masses will barely compress the cells and therefore not generate

enough deformation for potential energy to be stored and subsequently released. In these cases, the energy dissipation should approach 100%.

Our theoretical model so far may exceed 100% if s or d is large. To model the realistic case, we adopt the common method of using an envelope function E to bound the x equation stated in Eq. (1) based on our experimental data as follows:

$$E(x) = L(1 - \exp(-gx^{\frac{1}{p}})). \tag{2}$$

Here, L denotes the maximum loss possible in the system. The envelope function is an inverse exponential function with L and the two other constants g and p being determined by fitting the experiment data to the equation.

In our experiments, we care about the actual loss of the energy instead of the ratio of the energy loss so that we can use it in the visualization in the app. Therefore, our theory to be validated takes the following final form:

$$Loss[\text{in J}] = E(x) \times (\text{initial energy}), \tag{3}$$

where the initial energy is calculated as the gravitational potential energy of the ball, which is the product of the drop height, the mass, and the gravitational constant. We report all coefficients for our model in Table 1. To obtain these, we fit all experimental data to the formulation Eq. (3) using non-linear least squares fitting through Python's *SciPy* package[6]. Over all data points, we obtain a relative approximated residual of 3%.

Table 1: The coefficients yielded by fitting the experimental data to our model.

Coefficient	Value
k_s	0.01399
b_s	0.00800
k_d	2.19099×10^{-9}
b_d	0.00585
t	0.27467
p	0.96035
g	2.29619
L	0.93441

5.4 Configuration Editor

We support novice users in configuring their material by computing the number of active spring and damper cells in their material to help them achieve their desired configuration of elasticity. Our editor is focusing on computing and displaying the *dynamic* elastic features, such as predicting the bounce height of a user-defined mass. Given that users would have the generic metamaterial in stock, they can explore the static stiffness features (e.g., softness, tilting) easily in a hands-on manner. Our design tool is intended to help users create fine-tuned elastic areas for predictable dynamic responses that cannot easily be configured by end-users otherwise.

[6]https://docs.scipy.org/doc/scipy/

We built a simple Rhino-based configuration editor that allows users to define areas, indicate the desired bounce back height, and the approximate mass. Using these parameters, we compute which cells should be active, give users a simple preview by simulating a bouncing ball, and generate the geometry for users to 3D print. We use our previously introduced model to predict the returned energy and build a brute-force algorithm that computes distribution of spring and damper cells.

As shown in Fig. 19, users define the patch size by numbers of cells, the mass they intend to use and the bounce back they aim for. Since our model is not monotonous, we search through the feasible space. Our brute-force algorithm iteratively traverses the combinations, starting with one spring and looping through all available dampers. This is repeated until all possible springs have been evaluated. For each spring-damper combination, we keep track of the one with the minimum residual error in the bounce back height. By doing so, we keep the configuration that is closest to the desired bounce height. Our model facilitates a fast prediction such that the coupled cells are updated in real-time.

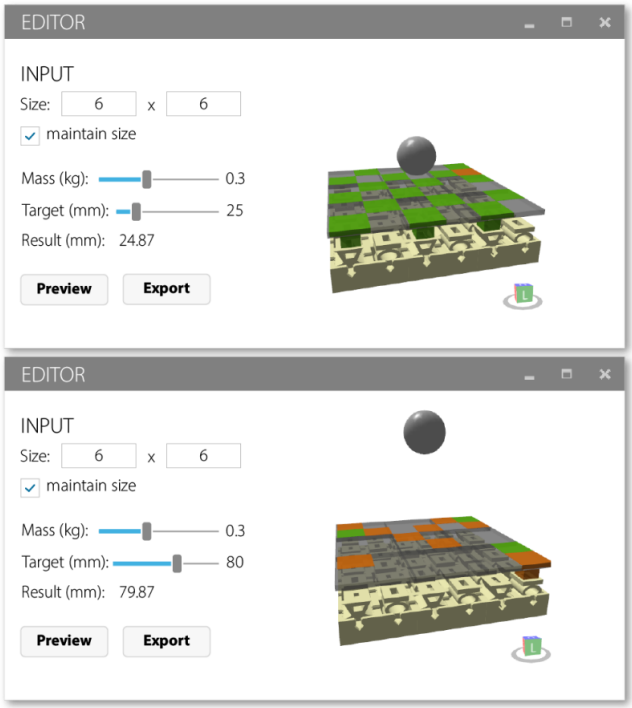

Figure 19: Our editor allows users to define their material's elasticity. Users can define the patch size, the mass they intend to use and the target bounce height relative to a drop height of 330 mm. Our algorithm computes the number of cells and distributes them evenly across the material. Users can preview the bouncing ball and export the 3D printable configuration layer geometry as STL.

6 DISCUSSION & LIMITATIONS

Deform. We mainly focused on flat sheets in this paper. Given that the generic material is deformable, it can also be wrapped around cylindrical objects. In that case, the coupling of cells would be constrained to row-wise coupling given that the configuration lids are rigid. Additionally, the flat surface of the configuration layer can be customized by modeling 2.5D or 3D shapes onto it. The generic metamaterial can be cut to shape at its flexible connections. To extend the metamaterial to large sheets, users can utilize snaps that are similar to the deformation lock, which allows for a repeatable configuration.

Properties & Range. Our metamaterial can, by design, span elastic and compliance properties. The elastic behavior can be tuned from behaving like a spring to damper within a range that is determined by the cells' stiffness and the coupled area. Not coupling cells results in a material that feels soft, while increasing the number of coupled cells yields materials that can be tuned to feel increasingly rigid, as shown in our VR seat example (Fig. 6b).

The scale of the material dictates the stiffness of the cells and consequently the range of mass it is effective for. We show the different scales used across our applications in Fig. 7c. The smallest version is 15 mm and with a spring stiffness of 1000 N/m best suited for handheld applications, e. g., the VR remote and hand pump, or the piano. The large cells (30 mm) are applicable for human-scale loads, as we show in the VR seating example. The mid-scale cells of 22.5 mm performed best for our ball game example given the heavy 250 g ball and the dynamic impact forces.

Evaluation. Our evaluation used only our default cell size of 22.5 mm, so our model might be biased for this data set. We would like to perform further evaluation in the future, to include different cell sizes and even multiple layers of such materials as that will expand the tuning capabilities further.

Durability & Miniaturization. While a formal durability test is pending, we designed our metamaterial with durability in mind. We designed our cells to remain in their rest-shape when no force is applied, which mitigates effects of material fatigue. After 2 months of experiments, we did not observe any significant change in performance. Additionally, the rubber-like base material we chose in our current research prototypes is a highly durable elastomer (Ninjaflex TPU, 65% elongation at yield, 660% elongation at break). We envision that our generic metamaterial could be industrially fabricated in smaller scales in the future. Similar base materials should be used for smaller-scale versions to maintain similar properties as our research prototypes.

7 CONCLUSION

We presented a concept for reconfigurable metamaterials by end-users. The main benefits arise from the decomposition of the material into a (1) generic, complex, industrially fabricated material and a (2) simple configuration geometry that is easy to fabricate with readily available materials by end-users. In this paper specifically, we investigated *elasticity* as the reconfigurable property of our metamaterial. We introduced design for two cells, i. e., spring and damper cells, that are arranged in a checkerboard pattern across the generic material. We evaluated and modeled their performance and implemented a simple configuration editor to assist users. We demonstrate the potential applicability of our metamaterial with various examples, including as augmentation for haptic props in VR, customizable shoe soles based on the users' activities, or a piano with customized stiffness. Note that by altering the arrangement of the active cells, we showed simple tilting mechanisms and by configuring how the frames are locked we can adapt to various shapes.

Based on the design choice of keeping a generic material (always in yellow) and only changing its function by fabricating specific, simple parts from rigid materials (in black), we believe that this material could be mass-manufactured, e. g., by row-wise extrusion. While we have not formally evaluated the durability of the generic material, we believe that it would hold up well since the cells remain in their rest state between use.

In the future, we seek to expand the range of properties that can be reconfigured and employ miniaturize versions for precision mechanisms, robotics, or electronics.

ACKNOWLEDGMENTS

This project was supported by Carnegie Mellon University's GSA/ Provost GuSH Grant funding. We thank David Lindlbauer for building the VR environment for our demo and insightful discussions.

REFERENCES

[1] Lea Albaugh, James McCann, Scott E. Hudson, and Lining Yao. 2021. *Engineering Multifunctional Spacer Fabrics Through Machine Knitting.* Association for Computing Machinery, New York, NY, USA. https://doi.org/10.1145/3411764.3445564

[2] Byoungkwon An, Ye Tao, Jianzhe Gu, Tingyu Cheng, Xiang 'Anthony' Chen, Xiaoxiao Zhang, Wei Zhao, Youngwook Do, Shigeo Takahashi, Hsiang-Yun Wu, Teng Zhang, and Lining Yao. 2018. *Thermorph: Democratizing 4D Printing of Self-Folding Materials and Interfaces.* Association for Computing Machinery, New York, NY, USA, 1–12. https://doi.org/10.1145/3173574.3173834

[3] Jatin Arora, Aryan Saini, Nirmita Mehra, Varnit Jain, Shwetank Shrey, and Aman Parnami. 2019. VirtualBricks: Exploring a Scalable, Modular Toolkit for Enabling Physical Manipulation in VR. In *Proceedings of the 2019 CHI Conference on Human Factors in Computing Systems* (Glasgow, Scotland Uk) *(CHI '19).* Association for Computing Machinery, New York, NY, USA, 1–12. https://doi.org/10.1145/3290605.3300286

[4] Katia Bertoldi, Vincenzo Vitelli, Johan Christensen, and Martin Van Hecke. 2017. Flexible mechanical metamaterials. *Nature Reviews Materials* 2, 11 (2017), 1–11.

[5] Bernd Bickel, Moritz Bächer, Miguel A Otaduy, Hyunho Richard Lee, Hanspeter Pfister, Markus Gross, and Wojciech Matusik. 2010. Design and fabrication of materials with desired deformation behavior. *ACM Transactions on Graphics (TOG)* 29, 4 (2010), 1–10.

[6] Tiemo Bückmann, Michael Thiel, Muamer Kadic, Robert Schittny, and Martin Wegener. 2014. An elasto-mechanical unfeelability cloak made of pentamode metamaterials. *Nature communications* 5, 1 (2014), 1–6.

[7] Paolo Celli, Connor McMahan, Brian Ramirez, Anton Bauhofer, Christina Naify, Douglas Hofmann, Basile Audoly, and Chiara Daraio. 2018. Shape-morphing architected sheets with non-periodic cut patterns. *Soft matter* 14, 48 (2018), 9744–9749.

[8] Desai Chen, David I. W. Levin, Wojciech Matusik, and Danny M. Kaufman. 2017. Dynamics-Aware Numerical Coarsening for Fabrication Design. *ACM Trans. Graph.* 36, 4, Article 84 (July 2017), 15 pages. https://doi.org/10.1145/3072959.3073669

[9] Desai Chen, Mélina Skouras, Bo Zhu, and Wojciech Matusik. 2018. Computational discovery of extremal microstructure families. *Science advances* (2018).

[10] Tian Chen, Mark Pauly, and Pedro M Reis. 2021. A reprogrammable mechanical metamaterial with stable memory. *Nature* 589, 7842 (2021), 386–390.

[11] Tian Chen and Kristina Shea. 2016. Design and Fabrication of Hierarchical Multi-Stable Structures Through Multi-Material Additive Manufacturing *(International Design Engineering Technical Conferences and Computers and Information in Engineering Conference, Vol. Volume 2A: 42nd Design Automation Conference).* https://doi.org/10.1115/DETC2016-59856

[12] Jack Forman, Mustafa Doga Dogan, Hamilton Forsythe, and Hiroshi Ishii. 2020. DefeXtiles: 3D Printing Quasi-Woven Fabric via Under-Extrusion. In *Proceedings of the 33rd Annual ACM Symposium on User Interface Software and Technology*

(Virtual Event, USA) *(UIST '20)*. Association for Computing Machinery, New York, NY, USA, 1222–1233. https://doi.org/10.1145/3379337.3415876

[13] Tobias Frenzel, Claudio Findeisen, Muamer Kadic, Peter Gumbsch, and Martin Wegener. 2016. Tailored Buckling Microlattices as Reusable Light-Weight Shock Absorbers. *Advanced Materials* 28, 28 (2016), 5865–5870. https://doi.org/10.1002/adma.201600610

[14] Jun Gong, Olivia Seow, Cedric Honnet, Jack Forman, and Stefanie Mueller. 2021. MetaSense: Integrating Sensing Capabilities into Mechanical Metamaterial *(UIST '21)*. Association for Computing Machinery, New York, NY, USA, 1063–1073. https://doi.org/10.1145/3472749.3474806

[15] Babak Haghpanah, Hamid Ebrahimi, Davood Mousanezhad, Jonathan Hopkins, and Ashkan Vaziri. 2015. Programmable Elastic Metamaterials. *Advanced Engineering Materials* 18, 4 (2015), 643–649. https://doi.org/10.1002/adem.201500295

[16] Babak Haghpanah, Ladan Salari-Sharif, Peyman Pourrajab, Jonathan Hopkins, and Lorenzo Valdevit. 2016. Multistable Shape-Reconfigurable Architected Materials. *Advanced Materials* 28, 36 (2016), 7915–7920. https://doi.org/10.1002/adma.201601650

[17] Adli Haron and K A Ismail. 2012. Coefficient of restitution of sports balls: A normal drop test. *IOP Conference Series: Materials Science and Engineering* 36 (sep 2012), 012038. https://doi.org/10.1088/1757-899x/36/1/012038

[18] Liang He, Gierad Laput, Eric Brockmeyer, and Jon E. Froehlich. 2017. SqueezaPulse: Adding Interactive Input to Fabricated Objects Using Corrugated Tubes and Air Pulses. In *Proceedings of the Eleventh International Conference on Tangible, Embedded, and Embodied Interaction* (Yokohama, Japan) *(TEI '17)*. Association for Computing Machinery, New York, NY, USA, 341–350. https://doi.org/10.1145/3024969.3024976

[19] Liang He, Huaishu Peng, Michelle Lin, Ravikanth Konjeti, François Guimbretière, and Jon E. Froehlich. 2019. Ondulé: Designing and Controlling 3D Printable Springs. In *Proceedings of the 32nd Annual ACM Symposium on User Interface Software and Technology* (New Orleans, LA, USA) *(UIST '19)*. Association for Computing Machinery, New York, NY, USA, 739–750. https://doi.org/10.1145/3332165.3347951

[20] Anuruddha Hettiarachchi and Daniel Wigdor. 2016. Annexing Reality: Enabling Opportunistic Use of Everyday Objects as Tangible Proxies in Augmented Reality. In *Proceedings of the 2016 CHI Conference on Human Factors in Computing Systems* (San Jose, California, USA) *(CHI '16)*. Association for Computing Machinery, New York, NY, USA, 1957–1967. https://doi.org/10.1145/2858036.2858134

[21] Scott E. Hudson. 2014. Printing Teddy Bears: A Technique for 3D Printing of Soft Interactive Objects. In *Proceedings of the SIGCHI Conference on Human Factors in Computing Systems* (Toronto, Ontario, Canada) *(CHI '14)*. Association for Computing Machinery, New York, NY, USA, 459–468. https://doi.org/10.1145/2556288.2557338

[22] Alexandra Ion, Johannes Frohnhofen, Ludwig Wall, Robert Kovacs, Mirela Alistar, Jack Lindsay, Pedro Lopes, Hsiang-Ting Chen, and Patrick Baudisch. 2016. Metamaterial Mechanisms. In *Proceedings of the 29th Annual Symposium on User Interface Software and Technology* (Tokyo, Japan) *(UIST '16)*. Association for Computing Machinery, New York, NY, USA, 529–539. https://doi.org/10.1145/2984511.2984540

[23] Alexandra Ion, Robert Kovacs, Oliver S. Schneider, Pedro Lopes, and Patrick Baudisch. 2018. Metamaterial Textures. In *Proceedings of the 2018 CHI Conference on Human Factors in Computing Systems* (Montreal QC, Canada) *(CHI '18)*. Association for Computing Machinery, New York, NY, USA, 1–12. https://doi.org/10.1145/3173574.3173910

[24] Alexandra Ion, David Lindlbauer, Philipp Herholz, Marc Alexa, and Patrick Baudisch. 2019. Understanding Metamaterial Mechanisms. In *Proceedings of the 2019 CHI Conference on Human Factors in Computing Systems* (Glasgow, Scotland Uk) *(CHI '19)*. Association for Computing Machinery, New York, NY, USA, 1–14. https://doi.org/10.1145/3290605.3300877

[25] Alexandra Ion, Ludwig Wall, Robert Kovacs, and Patrick Baudisch. 2017. Digital Mechanical Metamaterials. In *Proceedings of the 2017 CHI Conference on Human Factors in Computing Systems* (Denver, Colorado, USA) *(CHI '17)*. Association for Computing Machinery, New York, NY, USA, 977–988. https://doi.org/10.1145/3025453.3025624

[26] Jeeeun Kim, Qingnan Zhou, Amanda Ghassaei, and Xiang 'Anthony' Chen. 2021. OmniSoft: A Design Tool for Soft Objects by Example. In *Proceedings of the Fifteenth International Conference on Tangible, Embedded, and Embodied Interaction* (Salzburg, Austria) *(TEI '21)*. Association for Computing Machinery, New York, NY, USA, Article 15, 13 pages. https://doi.org/10.1145/3430524.3440634

[27] Daniel Kleppner and Robert Kolenkow. 2014. *An Introduction to Mechanics*. Cambridge University Press.

[28] Donghyeon Ko, Jee Bin Yim, Yujin Lee, Jaehoon Pyun, and Woohun Lee. 2021. Designing Metamaterial Cells to Enrich Thermoforming 3D Printed Object for Post-Print Modification. In *Proceedings of the 2021 CHI Conference on Human Factors in Computing Systems* (Yokohama, Japan) *(CHI '21)*. Association for Computing Machinery, New York, NY, USA, Article 671, 12 pages. https://doi.org/10.1145/3411764.3445229

[29] Robert Kovacs, Alexandra Ion, Pedro Lopes, Tim Oesterreich, Johannes Filter, Philipp Otto, Tobias Arndt, Nico Ring, Melvin Witte, Anton Synytsia, and Patrick Baudisch. 2018. TrussFormer: 3D Printing Large Kinetic Structures. In *Proceedings of the 31st Annual ACM Symposium on User Interface Software and Technology* (Berlin, Germany) *(UIST '18)*. Association for Computing Machinery, New York, NY, USA, 113–125. https://doi.org/10.1145/3242587.3242607

[30] Roderic Lakes. 1987. Foam structures with a negative Poisson's ratio. *Science* 235 (1987), 1038–1041.

[31] Jonàs Martínez, Haichuan Song, Jérémie Dumas, and Sylvain Lefebvre. 2017. Orthotropic k-Nearest Foams for Additive Manufacturing. *ACM Trans. Graph.* 36, 4, Article 121 (July 2017), 12 pages. https://doi.org/10.1145/3072959.3073638

[32] MJ Mirzaali, Shahram Janbaz, M Strano, L Vergani, and Amir A Zadpoor. 2018. Shape-matching soft mechanical metamaterials. *Scientific reports* 8, 1 (2018), 1–7.

[33] Lauren C Montemayor, Lucas R Meza, and Julia R Greer. 2014. Design and Fabrication of Hollow Rigid Nanolattices via Two-P hoton Lithography. *Advanced Engineering Materials* 16, 2 (2014), 184–189.

[34] Jifei Ou, Mélina Skouras, Nikolaos Vlavianos, Felix Heibeck, Chin-Yi Cheng, Jannik Peters, and Hiroshi Ishii. 2016. AeroMorph - Heat-Sealing Inflatable Shape-Change Materials for Interaction Design. In *Proceedings of the 29th Annual Symposium on User Interface Software and Technology* (Tokyo, Japan) *(UIST '16)*. Association for Computing Machinery, New York, NY, USA, 121–132. https://doi.org/10.1145/2984511.2984520

[35] Johannes TB Overvelde, Twan A De Jong, Yanina Shevchenko, Sergio A Becerra, George M Whitesides, James C Weaver, Chuck Hoberman, and Katia Bertoldi. 2016. A three-dimensional actuated origami-inspired transformable metamaterial with multiple degrees of freedom. *Nature communications* 7, 1 (2016), 1–8.

[36] Julian Panetta, Qingnan Zhou, Luigi Malomo, Nico Pietroni, Paolo Cignoni, and Denis Zorin. 2015. Elastic Textures for Additive Fabrication. *ACM Trans. Graph.* 34, 4, Article 135 (July 2015), 12 pages. https://doi.org/10.1145/2766937

[37] Huaishu Peng, Jennifer Mankoff, Scott E. Hudson, and James McCann. 2015. A Layered Fabric 3D Printer for Soft Interactive Objects. In *Proceedings of the 33rd Annual ACM Conference on Human Factors in Computing Systems*. Association for Computing Machinery, New York, NY, USA, 1789–1798. https://doi.org/10.1145/2702123.2702327

[38] Ahmad Rafsanjani and Katia Bertoldi. 2017. Buckling-Induced Kirigami. *Phys. Rev. Lett.* 118 (Feb 2017), 084301. Issue 8. https://doi.org/10.1103/PhysRevLett.118.084301

[39] Thomasa Reppel and Kerstin Weinberg. 2018. Experimental determination of elastic and rupture properties of printed Ninjaflex. *Technische Mechanik-European Journal of Engineering Mechanics* 38, 1 (2018), 104–112.

[40] Daniel J. Riddoch, Alice Cicirello, and David A. Hills. 2020. Response of a mass-spring system subject to Coulomb damping and harmonic base excitation. *International Journal of Solids and Structures* 193-194 (2020), 527–534. https://doi.org/10.1016/j.ijsolstr.2020.02.037

[41] Michael L. Rivera and Scott E. Hudson. 2019. *Desktop Electrospinning: A Single Extruder 3D Printer for Producing Rigid Plastic and Electrospun Textiles*. Association for Computing Machinery, New York, NY, USA, 1–12. https://doi.org/10.1145/3290605.3300434

[42] Michael L. Rivera, Melissa Moukperian, Daniel Ashbrook, Jennifer Mankoff, and Scott E. Hudson. 2017. *Stretching the Bounds of 3D Printing with Embedded Textiles*. Association for Computing Machinery, New York, NY, USA, 497–508. https://doi.org/10.1145/3025453.3025460

[43] Rei Sakura, Changyo Han, Keisuke Watanabe, Ryosuke Yamamura, and Yasuaki Kakehi. 2022. Design of 3D-Printed Soft Sensors for Wire Management and Customized Softness. In *Extended Abstracts of the 2022 CHI Conference on Human Factors in Computing Systems* (New Orleans, LA, USA) *(CHI EA '22)*. Association for Computing Machinery, New York, NY, USA, Article 192, 5 pages. https://doi.org/10.1145/3491101.3519906

[44] Valkyrie Savage, Andrew Head, Björn Hartmann, Dan B. Goldman, Gautham Mysore, and Wilmot Li. 2015. *Lamello: Passive Acoustic Sensing for Tangible Input Components*. Association for Computing Machinery, New York, NY, USA, 1277–1280. https://doi.org/10.1145/2702123.2702207

[45] Krishna Kumar Saxena, Raj Das, and Emilio P. Calius. 2016. Three Decades of Auxetics Research – Materials with Negative Poisson's Ratio: A Review. *Advanced Engineering Materials* 18, 11 (2016), 1847–1870. https://doi.org/10.1002/adem.201600053

[46] Christian Schumacher, Bernd Bickel, Jan Rys, Steve Marschner, Chiara Daraio, and Markus Gross. 2015. Microstructures to Control Elasticity in 3D Printing. *ACM Trans. Graph.* 34, 4, Article 136 (July 2015), 13 pages. https://doi.org/10.1145/2766926

[47] Sicong Shan, Sung H. Kang, Jordan R. Raney, Pai Wang, Lichen Fang, Francisco Candido, Jennifer A. Lewis, and Katia Bertoldi. 2015. Multistable Architected Materials for Trapping Elastic Strain Energy. *Advanced Materials* 27, 29 (2015), 4296–4301. https://doi.org/10.1002/adma.201501708

[48] Madlaina Signer, Alexandra Ion, and Olga Sorkine-Hornung. 2021. Developable Metamaterials: Mass-Fabricable Metamaterials by Laser-Cutting Elastic Structures. In *Proceedings of the 2021 CHI Conference on Human Factors in Computing Systems* (Yokohama, Japan) *(CHI '21)*. Association for Computing Machinery, New York, NY, USA, Article 674, 13 pages. https://doi.org/10.1145/3411764.3445666

[49] Ronit Slyper, Ivan Poupyrev, and Jessica Hodgins. 2011. Sensing through Structure: Designing Soft Silicone Sensors. In *Proceedings of the Fifth International Conference on Tangible, Embedded, and Embodied Interaction* (Funchal, Portugal) *(TEI '11)*. Association for Computing Machinery, New York, NY, USA, 213–220. https://doi.org/10.1145/1935701.1935744

[50] Haruki Takahashi and Jeeeun Kim. 2019. 3D Printed Fabric: Techniques for Design and 3D Weaving Programmable Textiles. In *Proceedings of the 32nd Annual ACM Symposium on User Interface Software and Technology* (New Orleans, LA, USA) *(UIST '19)*. Association for Computing Machinery, New York, NY, USA, 43–51. https://doi.org/10.1145/3332165.3347896

[51] Guanyun Wang, Humphrey Yang, Zeyu Yan, Nurcan Gecer Ulu, Ye Tao, Jianzhe Gu, Levent Burak Kara, and Lining Yao. 2018. 4DMesh: 4D Printing Morphing Non-Developable Mesh Surfaces. In *Proceedings of the 31st Annual ACM Symposium on User Interface Software and Technology* (Berlin, Germany) *(UIST '18)*. Association for Computing Machinery, New York, NY, USA, 623–635. https://doi.org/10.1145/3242587.3242625

[52] Chen Yang, Manish Boorugu, Andrew Dopp, Jie Ren, Raymond Martin, Daehoon Han, Wonjoon Choi, and Howon Lee. 2019. 4D printing reconfigurable, deployable and mechanically tunable metamaterials. *Material Horizons* 6 (2019), 1244–1250. Issue 6. https://doi.org/10.1039/C9MH00302A

[53] Dian Yang, Bobak Mosadegh, Alar Ainla, Benjamin Lee, Fatemeh Khashai, Zhigang Suo, Katia Bertoldi, and George M. Whitesides. 2015. Buckling of Elastomeric Beams Enables Actuation of Soft Machines. *Advanced Materials* 27, 41 (2015), 6323–6327. https://doi.org/10.1002/adma.201503188